2019 International Conference on Indoor Positioning and Indoor Navigation (IPIN), 30 Sept. - 3 Oct. 2019, Pisa, Italy

Performance Analysis of a 60-GHz Radar for Indoor Positioning and Tracking

A. Antonucci*, M. Corrà†, A. Ferrari‡, D. Fontanelli§, E. Fusari†, D. Macii§, L. Palopoli*
*Dep. of Information Engineering and Computer Science, University of Trento, Italy, E–mail: alessandro.antonucci@unitn.it
†Tretec S.r.L., Trento, Italy, E–mail: michele.corra@3tec.it
‡VNG Ingegneria Trento, Italy, E–mail: alessandro.ferrari@vngingegneria.it
§Dep. of Industrial Engineering, University of Trento, Italy, E–mail: daniele.fontanelli@unitn.it

***Abstract*—Among the manifold wireless technologies recently adopted for indoor localization and tracking, radars based on phased-array transceivers at 60 GHz are gaining momentum. The main advantages of this technology are: high accuracy, good ability to track multiple target with a low computation burden and preservation of privacy. Despite the growing commercial success of low-cost radar platforms, accurate studies to evaluate their tracking performance are not frequent in the literature, the main reasons being the commercial policies that prevent a direct access to the processed data and the difficult calibration of indoor positioning systems under dynamic conditions. This paper aims to fill this gap providing an extensive and scientifically sound performance analysis of one of these sensors (i.e., the System-on-Chip (SOC) TI IWR6843) and exposing benefits and limitations of 60-GHz mm-wave sensors for people localization and tracking. Multiple experimental results show that the average standard positioning uncertainty is about 30 cm under dynamic conditions. Our study also reveals the critical impact of three parameters, which are not properly documented by the manufacturer. Localization accuracy and robustness are also significantly affected by the risk of delayed and spurious detections. In the paper, a possible mitigation strategy of these anomalies is presented.**

Keywords*—Indoor positioning, radar, 60-GHz transceivers, performance evaluation, uncertainty.

I. Introduction

Indoor localization and tracking of humans, robots and goods is essential for a large number of Information and Communication Technologies (ICT) applications. A largely incomplete list of such applications includes people counting, security monitoring, and trajectory planning or optimization for service robots [1]. The solutions adopted for localization and tracking take a different shape depending on the considered target type. When tracking a robot, it is possible to merge odometry and inertial sensors data with the information derived from visual landmarks or Radio Frequency Identification (RFID) tags with given coordinates in the considered reference frame [2]–[4]. When instead the entity to be localized and tracked is a human, data fusion can still be a possibility using different sensing technologies. For instance, it is possible to use wearable inertial platforms to estimate the user's relative motion and RF transceivers (preferably based on standard, widely available Wi-Fi or Bluetooth modules) to measure the distance from fixed anchor nodes [5]–[8]. Since the solutions based on Received Signal Strength Intensity (RSSI) from reference nodes (e.g., Wi-Fi access points) suffer from major spurious fluctuations in both time and space, alternative techniques based on low-level Time-of-Flight (ToF) measurements of Ultra-Wide Band (UWB) or Chirp Spread Spectrum (CSS) signals have been proposed [9]–[12]. UWB systems have been used for vital sign sensing as well as for near-field imaging applications since the early 2000s [13]. More recently UWB systems have been used to detect people trapped or behind walls [14]. Moreover, millimeter-wave (mm-wave) RF signals can be used to implement radars with a range of a few meters. Like surveillance cameras or other types of visual sensors [15], [16], mm-wave radars can be installed in strategic locations of a given environment and used to track target who are not required to carry any kind of electronic device. However, radars have a number of advantages compared with cameras, i.e.

1) They are cheaper and need simpler signal processing algorithms;
2) Target detection is more insensitive to obstructions;
3) People identity and privacy are preserved, as it is difficult to associate a cloud of points to a specific individual;
4) Radar signals are not affected by changing illumination conditions: they can operate indoor and outdoor regardless of light variations or changeable weather conditions.

Even if the idea of implementing low-cost radars for people localization traces back to more than 10 years ago [17], the solutions based on antenna arrays have evolved especially in the last few years as a result of the research activities on massive multiple-input multiple-output (MIMO) systems, particularly for 5G communications [18], [19]. For instance, in [20] a channel model for personal radar applications based on mm-wave antenna arrays is described and is used to scan the environment and to reconstruct a map of it. Moreover, in [21] the influence of different design parameters on mm-wave radar-based mapping performance is analyzed. Over the last few years, mm-wave RF signals have been used to localize and to track a moving target in a variety of ways, e.g., by using Angle-of-Arrival measurements, by combining path loss with Angle-of-Arrival data or through Angle Differences-of-Arrival algorithms [22], [23]. Since mm-wave radars operate at frequencies higher than 10 GHz [24], [25], arrays of small and closely spaced antennas can be easily implemented on the platform itself at a reduced cost and with a small footprint. In this case, the position of the target can be estimated from the Phase Differences of Arrival (PDoA) of the backscattered waveforms received by different antennas [26]. This general approach has been also used to implement low-cost commercial off-the-shelf

978-1-7281-1788-1/19/$31.00

Systems-on-Chip (SoCs) embedding both RF circuitry and digital signal processing algorithms for position estimation. However, the actual performance and the limitations of these platforms are still quite unclear. The information reported in the data sheets is usually partial or incomplete. In addition, a proper experimental characterization of these devices in dynamic conditions is hard to do and results are inaccurate or poorly presented. Thus, the main purpose of this paper is to fill this gap, taking a low-cost commercial mm-wave radar, namely the TI IWR6843 SoC, as a case study.

The rest of the paper is organized as follows. Section II summarizes the principle of operation of the radar-based platform and its main parameters of interest, although not all details are disclosed by the manufacturer. The static and dynamic performances of the system under test are reported in Section III. Since one of the main drawbacks of the system is the risk to have multiple spurious detection of the same target, in Section IV an algorithm to remove such outliers is described. Finally, in Section V the main conclusions are drawn and future work is outlined.

II. The radar-based positioning platform

The radar-based platform is based on an evaluation module comprising the TI IWR6843 SoC, an array composed by three transmitting and four receiving antennas and other electronic components to connect the SoC with other external systems. The evaluation module is placed in piggyback on a custom motherboard designed by Tretec S.r.L., Trento. The motherboard is equipped with an STM ARM Cortex-H7 microcontroller running at 256 MHz, 2 MB of flash memory and 1 MB of SRAM memory. The system is powered by a IEEE 802.3af Power over Ethernet class 1 interface that can drain about 300 mA on average at 3.3 V. Along with the Ethernet link, I/O connectivity is provided by 1 mini-USB port (for debug purposes), 2 RS-485 and 1 RS-232 ports and 3 independent I2C links. A task scheduler and the lightweight TCP/IP stack (lwIP v.2.0.3) have been properly customized for the firmware provided. SoC configuration and radar data streaming rely on a TCP/IP Ethernet connection. The IP address can be assigned either statically or dynamically (if a DHCP server is available). Remote system configuration as well as data acquisition and monitoring is performed via a Graphic User Interface (GUI) implemented in Java. A brief description of the radar-based positioning algorithm and its main configuration parameters is reported in the following.

A. Algorithm and SoC overview

The IWR6843 SoC relies on a Frequency Modulated Continuous Wave (FMCW) radar able to estimate the distance, the angle and the velocity of a moving target. FMCW radars transmit repeated frames of chirp signals using an antenna array and receive the backscattered ones with another one. The received and transmitted waveforms are mixed to produce an intermediate frequency (IF) signal, whose initial phase is given by the difference between the phases of the transmitted and received chirps. The distance between the target obstacle and the transceiver is a nonlinear function of this IF signal. The velocity measurements are obtained by transmitting equally spaced chirps and then by comparing the phases of two reflected ones estimated through the Fast Fourier Transform (FFT). A second FFT, called Doppler-FFT, is performed in order to resolve ambiguity between two moving targets. Finally, the angle can be estimated from the phase changes associated with the spectral magnitude peaks resulting from the FFT or the Doppler-FFT.

The IWR6843 SoC includes an ARM Cortex-R4F microcontroller (MCU) and a TI C674x Digital Signal Processor (DSP) acting as a co-processor for critical signal processing tasks. The people tracking algorithm running on the ARM Cortex-R4F is called once per frame, gets the measurement data in polar coordinates (range, angle, Doppler frequency shift), and returns the tracked objects in a Cartesian space. Since any target has a finite size and several chirps are transmitted and received at the same time by the antenna array, usually the distance from a multitude of points is measured at the same time. Such points may refer to the same or to different objects. Therefore, the points should be grouped accordingly. The algorithm relies on both an allocation and an association step. The allocation step creates sets of points (to be assigned to distinct possible targets) that do not belong to any already existing set. The allocation step is guided by some configuration parameters, as explained more in detail in Section II-B. The association step instead refers to the process of updating these sets, by keeping the previous points or adding the new ones that are closest to the corresponding centroid. An on-board extended Kalman filter (EKF) is used to track the position of the centroids resulting from the allocation and association steps.

B. Configuration parameters

The behavior of the detection and tracking algorithm embedded in the TI IWR6843 SoC depends on a variety of parameters. The *scenery* parameters, expressed in meters, define the limits of the detection area of the radar. Thus, all objects that lie outside such limits are not gathered into sets.

The *state transition* parameters determine the quickness with which each target in the allocation step starts or stops being tracked. The *state transition* settings, used in the static and dynamic tests described in Section III, are summarized below:

- A target is detected and starts being tracked as soon as the corresponding set of allocated points is steadily formed. This holds in both static and dynamic testing conditions;
- A target stops being tracked when the corresponding set of points disappears or stops moving for more than 50 or 500 algorithm iterations in dynamic or stationary conditions, respectively. Moreover, a target stops being tracked as soon as it exits the expected detection area.

Observe that, in the case of tests in stationary conditions, the threshold value adopted to halt tracking is 10 times larger than in the dynamic case, in order to prolong radar tracking ability as much as possible.

The *allocation* parameters guide the formation of the sets of points to be assigned to one or multiple targets. The most significant parameters of this kind will be labeled here and in the following as P_1 and P_2. The former one is an dimensionless threshold value used to discriminate possible

spurious points (typically due to background noise) from those that are associated to a moving target. In practice, with a higher value of P_1 the number of sets tends to decrease. As a consequence, the probability of missing actual targets increases. On the contrary, if P_1 decreases, the probability of spurious (i.e., false) detections grows. Parameter P_2 is instead a velocity threshold (expressed in m/s) representing the minimum radial velocity associated with the centroid of the set allocated to the same target.

Finally, the so-called *gating* parameters establish how and to what extent some detected points can be associated to one of the existing sets. The main parameter of this type (labeled as P_3 in the following) determines the maximum volume of a set. In practice, the points that are farther than P_3 from the centroid of a given set are considered not to belong to the corresponding target.

III. Setup description and experimental results

To test the performances of the radar-based platform, an experimental campaign was conducted in the laboratories of the University of Trento. The radar-based platform was fastened to a rigid support at about 2.30 m off the floor with a tilt angle of a few degrees. An OptiTrack Flex13 reference localization system equipped with 14 cameras Prime 13 (with a resolution of 1280×1024 pixels and a frame rate of 120 Hz) was used first to calibrate the radar-based platform in static conditions (namely, with a still target person) and then to measure the actual positions of one or two people moving along different paths. The trajectories estimated by the OptiTrack system can be regarded as the "ground truth", since the position of the ad-hoc reflective markers detected by OptiTrack can be measured with ± 1 mm accuracy. In the following subsections, first a description of the platform calibration procedure in static conditions and the related results are reported in Section III-A. Then, in Section III-B, the system behavior under dynamic conditions is analyzed.

A. Calibration procedure and results in static conditions

The nominal area over which the radar is supposed to detect a target is a sector of a circle with a radius of 6 m and with aperture angle of about 118°. However, some preliminary tests showed that the actual detection area is instead quite irregular and smaller than expected. In particular, we found that:

- In the longitudinal direction, the detection range spans from 0.46 m $\pm\, 0.09$ m to 5.55 m $\pm\, 0.12$ m;
- In the transverse direction, the left and right detection ranges are 1.91 m $\pm\, 0.05$ m and 3.04 m $\pm\, 0.36$ m, respectively.

Possible setup-related uncertainty contributions that need to be properly compensated (or at least mitigated) for a better characterization of the platform are:

1) The angular and translational systematic offsets between the reference frame associated with the OptiTrack and the frame of the radar-based system;
2) The misalignment between the timestamps of the data collected by both positioning systems;
3) The intrinsic difference between the points of the body selected by either system to identify the position of the target.

Given that the area monitored by the OptiTrack system is about 10 m $\times$ 7 m (i.e., quite larger than the radar range), the position and the orientation of the TI IWR6843 SoC was measured in the OptiTrack reference frame by placing three reflective markers on it. Hence, a roto-translational transformation was used to align the coordinates of the selected points in the reference frames of both positioning systems.

The uncertainty contributions due to timestamp misalignment were minimized by using the same PC to collect both OptiTrack and radar-based position data. Indeed, if the same PC clock is used for data time-stamping there is no need to synchronize the positioning systems. Since both the OptiTrack cameras and the radar-based platform stream their data to the PC through dedicated Ethernet cables linked to the same Ethernet switch and with a similar length, the communication delays differ by less than 10 ms. Therefore, their impact on target positioning accuracy at common pedestrian speeds (i.e., lower than 3 m/s) is in the order of a few centimeters.

Finally, as far as the third uncertainty contribution is concerned, the (x, y) coordinates of the target estimated by the OptiTrack and the values returned by the radar-based platform at the same time are likely to refer to different points of the body. This is due to the fact that to make the reflective markers detected by the OptiTrack visible from any position, they are placed on hats worn by users. Thus, the location of a target for the OptiTrack coincides with the position of user's head. On the contrary, the position estimates returned by the radar-based system coincide with those of the centroid of the cloud of points clustered by the algorithm running in the TI IWR684 SoC. Such a centroid is generally located within the trunk, although some fluctuations may occur due to the changes in distance and relative orientation between the user and the radar-based platform. In conclusion, a space-dependent geometric offset (in the order of some tens of cm) exist between the target positions measured by the OptiTrack and by the radar system, respectively. These offsets can be estimated and compensated through a bivariate linear regression applied to the points collected when a target is still in 9 different positions of the room, as shown in Fig. 1. The clusters of red points in Fig. 1 represent indeed the planar positions of the target measured by the radar-based platform in 1 minute for $P_1 = 375$, $P_2 = 0$ and $P_3 = 5$ (namely when the radar is maximally sensitive to target motion) *after* applying the calibration procedure based on the bivariate linear regression described above. Observe that the post-calibration residual offsets between the mean values of the (x, y) coordinates measured in each position and the corresponding ground-truth values (highlighted by blue circle markers) are negligible, which confirms that the calibration procedure is statistically correct. The average standard uncertainty along both axes is about 5 cm with some fluctuations that depend on the relative orientation between target and radar, as well as on the fact that a person must slightly swing to trigger radar detection.

B. Results in dynamic conditions

After platform calibration, multiple experiments have been conducted in dynamic conditions, i.e., with one or two targets

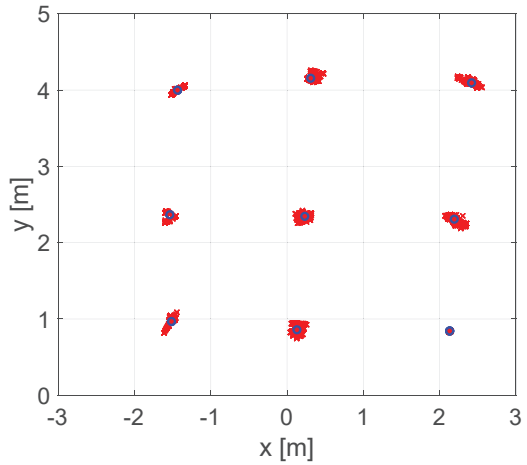

Fig. 1. Planar coordinates measured by the radar-based platform (red dots) in 9 different positions after the calibration procedure is applied. The blue circle markers represent the actual target's position, i.e. measured by the OptiTrack system.

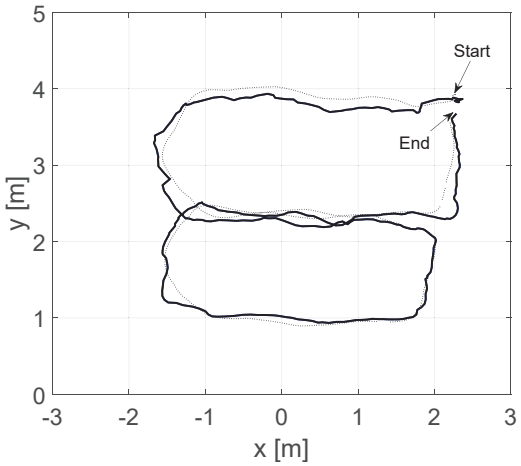

Fig. 2. Example of an eight-shaped path. Solid and dotted lines refer to the trajectories estimated by the radar-based platform and by the OptiTrack system, respectively.

moving straight (both longitudinally and transversally with respect to detection area of the radar), along eight-shaped paths or just randomly. For each type of trajectory, repeated experiments have been performed for 26 different triples of P_1, P_2 and P_3 values. Such triples have been selected with a trial-and-error approach and refer to the configurations for which the radar is responsive and measurement results are qualitatively reasonable. Fig. 2 displays an example of an eight-shaped trajectory estimated by the radar (solid line) for $P_1 = 500$, $P_2 = 0.5$ and $P_3 = 10$. The same trajectory estimated by the OptiTrack system (dotted line) is also shown for the sake of comparison. Observe that the average Euclidean positioning error in this case is about 14 cm.

The bar diagram in Fig. 3 shows the 99th percentiles of the relative positioning uncertainty $\gamma = \frac{d_r - d}{d}$ (where d_r and d are the distances of the target measured by the radar and by the OptiTrack system, respectively) as a function of the actual radial distance from the radar in three meaningful configurations.

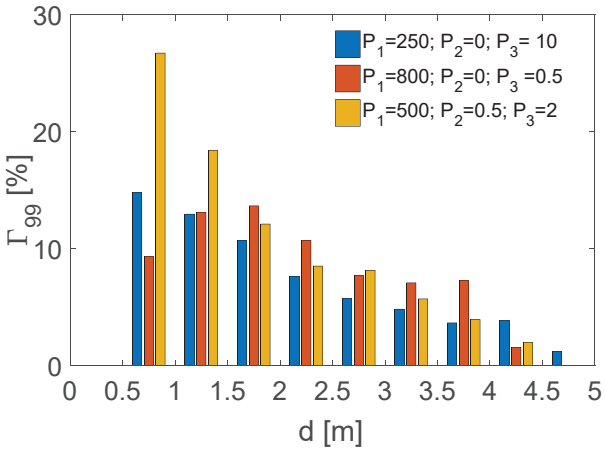

Fig. 3. 99th percentiles of the relative positioning uncertainty as a function of the actual distance from the radar for three different configurations of parameters P_1, P_2 and P_3.

Observe that globally the relative uncertainty tends to decrease with distance. Therefore, the absolute positioning uncertainty tends to be quite independent of d, which is consistent with the qualitative result shown in Fig. 2. However, by decreasing the value of P_1 and P_2 (which increases the sensitivity of the system, thus generating possible spurious detections) relative accuracy tends to improve.

Tab. I summarizes the results of the dynamic characterization of the radar-based platforms in different experiments. In particular, recalling that the *expanded uncertainty* is referred to as half of the width of the interval that is expected to encompass a given fraction of the values that can reasonably be attributed to a measurand [27], Tab. I reports the expanded uncertainties U_x and U_y (with coverage factor 2.7) associated with the measurement of the planar coordinates of the target when it moves over different kinds of paths and for several triples of P_1, P_2 and P_3 values. In practice, with the chosen coverage factor, the planar coordinates of a target lie in the intervals given by the (x, y) values measured by the radar-based platforms $\pm U_x$ and $\pm U_y$, respectively, with 99% confidence. Observe that in most configurations, the values of U_x and U_y range between 30 and 40 cm, with a few exceptions. Such results confirm that the radar-based localization is quite accurate. However, the rightmost column of Tab. I shows that for some configurations, a quite high percentage Q_S of spurious detections actually appears. In other words, while the probability of missing a target moving within the chosen detection area is negligible, multiple targets can be detected even when just one person is actually within the radar range. The reason of such a behavior is unclear at the moment, but it is definitely due to the detection algorithm running in the IWR6843 SoC. In particular, the probability of spurious detections greatly depends on P_1 and P_3 values (indeed Q_S suddenly increases when P_1 or P_3 become excessively low) and it is also affected by the kind of path. For instance, the aggregated results obtained with different parameters show that the probability of spurious detections is quite high in the case of straight paths (more than 22%), while it is 10% or less when the target moves randomly. It is worth emphasizing that sometimes the target was not detected and tracked immedi-

TABLE I. RESULTS OF THE DYNAMIC CHARACTERIZATION FOR DIFFERENT VALUES OF P_1, P_2 AND P_3. U_x AND U_y DENOTE THE EXPANDED UNCERTAINTIES (WITH COVERAGE FACTOR 2.7) ASSOCIATED WITH THE MEASUREMENT OF THE PLANAR COORDINATES OF THE TARGET WHEN IT MOVES OVER DIFFERENT PATHS. Q_S REPRESENTS INSTEAD THE FREQUENCY OF SPURIOUS TARGET DETECTIONS.

Conf.	Parameters			U_x [cm]	U_y [cm]	Q_S [%]
	P_1	P_2	P_3			
1	250	0	10	28	29	6.9
2	500	0	10	34	35	0
3	800	0	10	30	25	0
4	250	0.5	10	32	26	24
5	500	0.5	10	26	31	0
6	800	0.5	10	33	30	0
7	250	0.25	10	35	32	8.1
8	500	0.25	10	34	24	0
9	800	0.25	10	34	35	0
10	250	0	2	40	30	9.2
11	500	0	2	33	32	0
12	800	0	2	31	33	0
13	250	0.5	2	34	34	0
14	500	0.5	2	34	35	0
15	800	0.5	2	33	40	0
16	250	0.25	2	40	27	20.6
17	500	0.25	2	36	38	9.4
18	800	0.25	2	38	39	0
19	250	0	0.5	17	20	86.2
20	500	0	0.5	31	28	54.2
21	800	0	0.5	29	32	26.3
22	500	0.5	0.5	40	39	87.9
23	800	0.5	0.5	42	36	51.3
24	250	0.25	0.5	22	28	76.7
25	500	0.25	0.5	52	44	52.5
26	800	0.25	0.5	41	39	35.3

ately. The percentage of these events is particularly relevant (about 11 %) in the case of straight trajectories parallel to the $x-$axis, maybe because of the thinner shape of the sets of points clustered by the algorithm described in Section II-A when just a side of the target is observed. Notice that even if the radar-based platform is generally quite accurate, the risk of spurious detections sometimes can be very relevant. However, if P_1 and P_3 are set large enough, this risk becomes negligible.

IV. REJECTING SPURIOUS MEASUREMENTS

From the analysis carried out in Section III, it follows that for given particular values of the configuration parameters the radar occasionally provides spurious multiple target detections: besides the trajectory of the actual target, the algorithm returns additional points that are not related to any real object, but they are artifacts of the algorithm. Unfortunately, the system does not provide a direct access to the raw points generated by the SoC (at least using the firmware shipped with the device). For this reason, in case of multiple detections, we have developed an algorithm to create a ranking of different possible sets of points to decide which one is the most likely to refer to an actual target. The proposed algorithm is based on the combination of Kalman filtering and likelihood analysis.

First of all, from the paths estimated by the OptiTrack system, three different types of motion were identified: a) target standing still (H_0); b) target moving with a constant forward velocity (H_1); c) target moving with accelerated motion (H_2). For each one of these three kinds of motion, we developed a Kalman Filter (KF) whose model and the related parameters were set accordingly. In particular, the *Prediction Step* of each KF is given by

$$\begin{aligned} s^-_{i,k+1} &= A_i s_{i,k}, \\ \Sigma^-_{i,k+1} &= A_i \Sigma_{i,k} A_i^T + B_i Q B_i^T, \end{aligned} \tag{1}$$

where $i = 0, 1, 2$ denotes the H_0, H_1 and H_2 models, respectively, $s_{i,k}$ is the state of the i–th model at time step k and comprises the planar position, velocity and acceleration of the target within the chosen reference frame, whereas A_i is the system dynamic matrix of the i–th model. In particular, with reference to A_i, both target velocity and acceleration are zero for $i = 0$; the velocity is assumed to be constant and the acceleration is equal to zero for $i = 1$ and, finally, the acceleration is constant for $i = 2$. Moreover, $\Sigma_{i,k}$ is the covariance matrix of the estimation error associated with the i–th model at time step k, Q is the covariance matrix of the model uncertainties (assumed to be proportional to a perturbation in the acceleration space) and B_i is the uncertainties mapping matrix that enforce the constraints for the i–th model. Finally, the superscript $\cdot^-$ stands for the "predicted quantity".

In the *Update Step* of the KFs, the classic equations are used, i.e.

$$\begin{aligned} e_{i,k+1} &= z_{k+1} - C s^-_{i,k+1}, \\ S_{i,k+1} &= C \Sigma^-_{i,k+1} C^T + R, \\ K_{i,k+1} &= \Sigma^-_{i,k+1} C^T S^{-1}_{i,k+1}, \\ s_{i,k+1} &= s^-_{i,k+1} - K_{i,k+1} e_{i,k+1}, \\ \Sigma_{i,k+1} &= \Sigma^-_{i,k+1} - K_{i,k+1} C \Sigma^-_{i,k+1}, \end{aligned} \tag{2}$$

where z_{k+1} are the radar measurements collected at time $k+1$, R is the covariance matrix of the measurement uncertainty contributions and C is the output matrix of the model (notice that for each model we have the same matrix C, since only the position is measured). Moreover, $e_{i,k+1}$ is the innovation vector and $S_{i,k+1}$ is its covariance.

To select one of the possible three hypothesized motion models, i.e. H_0, H_1 and H_2, the Multiple Model Approach (MMA) presented in [28] is used. This approach provides a stochastic criterion for model selection. For instance, the probability of choosing the H_0 model at time $k+1$, i.e. $\mu_{0,k+1}$, is given by the Bayes' theorem, i.e.,

$$\mu_{0,k+1} = \frac{\Pr\left[z_{k+1} | H_0\right] \mu_{0,k}}{\Pr\left[z_{k+1}\right]}, \tag{3}$$

where $\Pr\left[z_{k+1} | H_0\right]$ is the likelihood of measuring z_{k+1} given the model H_0, which can be expressed as a Gaussian Probability Density Function (pdf) with mean $C s^-_{0,k+1}$ and covariance matrix $S_{0,k+1}$, both reported in (2). Note that the estimates $s_{0,k+1}$, $s_{1,k+1}$ and $s_{2,k+1}$ returned by the three filters are computed independently. While this is sufficient to converge to the correct probability when the system does not change its dynamic over time, this cannot be ruled out in the problem at hand. To account for potential mode changes, a first-order generalized pseudo-Bayesian estimator is adopted [28]. In this way, the estimates of each model are fused together in a single estimate before the *Prediction Step* associated with each model starts over. More precisely, the fused estimate and the

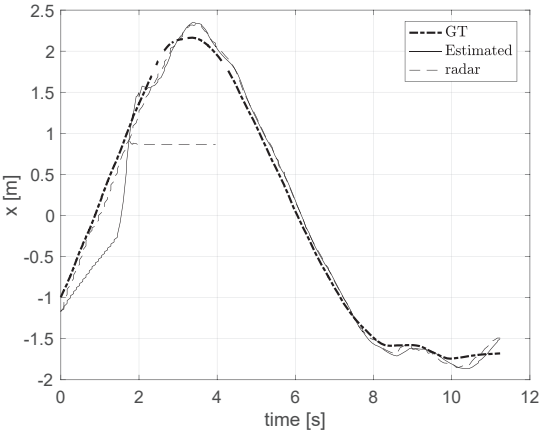

(a)

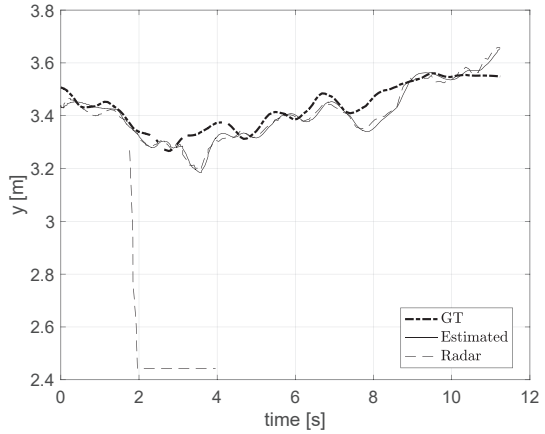

(b)

Fig. 4. Ground truth data (dash-dotted line), estimated trajectory (solid line) and radar measurements (dashed line) associates with the $x-$axis (a) and $y-$axis (b). Observe the spurious readings from about 2 s to 4 s.

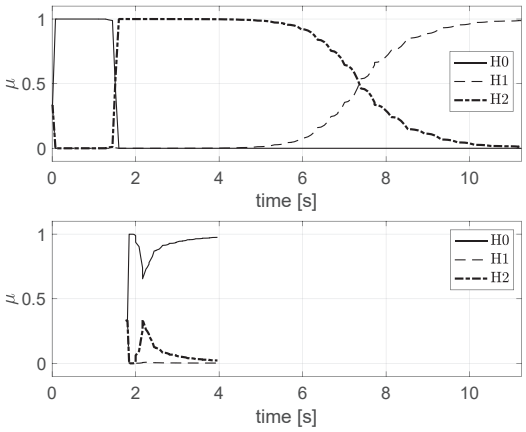

Fig. 5. Probabilities of the three models H_0, H_1 and H_2 in the case of correct (top) and spurious (bottom) target detection. This probabilities corresponds to the coordinates shown in Fig. 4.

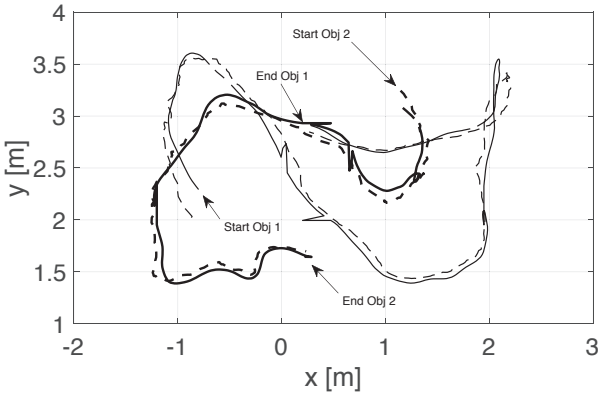

Fig. 6. Ground truth data (solid lines) and radar measured trajectories (dashed lines) of two human beings (identified with thick or thin lines) moving randomly in the radar detection area.

corresponding covariance matrix are given by

$$s_{k+1} = \sum_{i=0}^{2} \mu_{i,k+1} s_{i,k+1},$$
$$\Sigma_{k+1} = \sum_{i=0}^{2} \mu_{i,k+1} \left(\Sigma_{i,k+1} + [s_{k+1} - s_{i,k+1}][s_{k+1} - s_{i,k+1}]^T \right). \quad (4)$$

Again, due to the peculiarity of the system considered, this approach has a bias towards model H_0. Indeed, since the sampling period of the radar measurements is quite short compared to the typical time constants of human motion, the sampled data will be very close in space and, consequently, the likelihood will be favorable to the model with the target standing still. To overcome this limitation, the fusion is performed only after some consecutive measures (e.g., 5) are collected. With this filter hacking entirely due to typical human motion dynamic versus sampling time of the sensor, the presented approach is quite efficient in classifying the human dynamic with respect to models H_0, H_1 and H_2. To reject the spurious measurements, two further assumptions are considered: i) whenever multiple measurements are detected, the first-order generalized pseudo-Bayesian estimator is applied to the ensemble of the measured trajectories; ii) based on experimental evidence, we define as a spurious false detection, any trajectory that converges to H_0 while at least another one is classified either as H_1 or H_2. Using this simple heuristic criterion, most of spurious detections can be removed, as shown in Fig. 4. Indeed, the estimated trajectory (solid line) follows the ground truth data (dash-dotted line) regardless of the spurious data between 2 s and 4 s. This behavior is due to the correct identification of spurious multiple detections, as evident from the probabilities of each model related to the two trajectories (the correct and the spurious one) shown in Fig. 5.

Indeed, the top graph of Fig. 5 displays the probability that the first radar trajectory is classified either as H_1 or H_2. Observe that such a probability is generally 1 except at the very beginning. On the contrary, when the spurious trajectory comes into play (just before 2 s), this is correctly classified as H_0 and removed accordingly.

When two targets are tracked, the radar performances are similar to those shown in in Tab. I. Also, the effectiveness of the algorithm developed to detect and to remove possible spurious targets is comparable to the single target case. For a qualitative analysis, Fig. 6 reports an example with two

human beings moving randomly in the radar detection area. While these results are encouraging, further experiments with an increasing number of targets are needed to evaluate the scalability of the proposed solution.

V. Conclusions

Millimeter-wave (mm-wave) radars based on arrays of small and closely spaced antennas are currently among the most advanced solutions for accurate RF indoor localization and tracking. In this paper, the tracking performances of a last-generation commercial module, namely the TI IWR6843 SoC, have been evaluated in a variety of conditions using a high-accuracy optical tracking infrastructure as a reference. The experimental results lead to multi-faceted conclusions. The radar system generally ensures a planar positioning uncertainty (with 99% confidence level) in the order of 30-40 cm, which is acceptable for a large class of applications. However, the tracking algorithm running in the SoC is quite sensitive to the values of several of parameters that, in some conditions, lead to anomalies such as multiple spurious detections of the same user. A careful choice of the parameters can drastically reduce the frequency of these events. Moreover, it is possible to further mitigate this problem by adopting a Multiple Model Approach supported by a heuristic criterion.

Future research directions will be focused on the analysis of the sensing system and the proposed algorithms effectiveness in the case of multiple targets, i.e. when occlusions may occur along the tracking. Furthermore, we are planning to mount the radar on a moving platform to investigate its suitability for robotics applications.

References

[1] C. Laoudias, A. Moreira, S. Kim, S. Lee, L. Wirola, and C. Fischione, "A survey of enabling technologies for network localization, tracking, and navigation," *IEEE Communications Surveys Tutorials*, vol. 20, no. 4, pp. 3607–3644, Fourth quarter 2018.

[2] P. Nazemzadeh, D. Fontanelli, D. Macii, and L. Palopoli, "Indoor Localization of Mobile Robots through QR Code Detection and Dead Reckoning Data Fusion," *IEEE/ASME Transactions on Mechatronics*, vol. 22, no. 6, pp. 2588–2599, Dec. 2017.

[3] V. Kulyukin, A. Kutiyanawala, E. LoPresti, J. Matthews, and R. Simpson, "iWalker: Toward a rollator-mounted wayfinding system for the elderly," in *Proc. IEEE Int. Conference on RFID*, Las Vegas, NV, USA, Apr. 2008, pp. 303–311.

[4] P. Nazemzadeh, F. Moro, D. Fontanelli, D. Macii, and L. Palopoli, "Indoor Positioning of a Robotic Walking Assistant for Large Public Environments," *IEEE Trans. on Instrumentation and Measurement*, vol. 64, no. 11, pp. 2965–2976, Nov. 2015.

[5] A. Colombo, D. Fontanelli, D. Macii, and L. Palopoli, "Flexible Indoor Localization and Tracking based on a Wearable Platform and Sensor Data Fusion," *IEEE Trans. on Instrumentation and Measurement*, vol. 63, no. 4, pp. 864–876, Apr. 2014.

[6] W. Kang and Y. Han, "SmartPDR: Smartphone-based pedestrian dead reckoning for indoor localization," *IEEE Sensors Journal*, vol. 15, no. 5, pp. 2906–2916, May 2015.

[7] H. S. Maghdid, A. Al-Sherbaz, N. Aljawad, and I. A. Lami, "UNILS: Unconstrained indoors localization scheme based on cooperative smartphones networking with onboard inertial, bluetooth and gnss devices," in *Proc. 2016 IEEE/ION Position, Location and Navigation Symposium (PLANS)*, Savannah, GA, USA, Apr. 2016, pp. 129–136.

[8] D. Giovanelli, E. Farella, D. Fontanelli, and D. Macii, "Bluetooth-based Indoor Positioning through ToF and RSSI Data Fusion," in *Proc. International Conference on Indoor Positioning and Indoor Navigation (IPIN)*, Nantes, France, Sep. 2018, pp. 1–8.

[9] H. Hur and H. Ahn, "A circuit design for ranging measurement using chirp spread spectrum waveform," *IEEE Sensors Journal*, vol. 10, no. 11, pp. 1774–1778, Nov. 2010.

[10] C. Rohrig and L. Telle, "Real-time communication and localization for a swarm of mobile robots using ieee 802.15.4a css," in *2011 IEEE Vehicular Technology Conference (VTC Fall)*, San Francisco, CA, USA, Sep. 2011, pp. 1–5.

[11] C. Loyez, N. Rolland, and M. Bocquet, "Uwb technology applied to millimeter-wave indoor location systems," in *Proc. 2014 International Radar Conference*, Lille, France, Oct. 2014, pp. 1–5.

[12] G. De Angelis, A. Moschitta, and P. Carbone, "Positioning techniques in indoor environments based on stochastic modeling of UWB round-trip-time measurements," *IEEE Transactions on Intelligent Transportation Systems*, vol. 17, no. 8, pp. 2272–2281, Aug. 2016.

[13] D. M. Sheen, D. L. McMakin, and T. E. Hall, "Near field imaging at microwave and millimeter wave frequencies," in *Proc. 2007 IEEE/MTT-S International Microwave Symposium*, Honolulu, HI, USA, Jun. 2007, pp. 1693–1696.

[14] M. Loschonsky, C. Feige, O. Rogall, S. Fisun, and L. M. Reindl, "Detection technology for trapped and buried people," in *Proc. 2009 IEEE MTT-S International Microwave Workshop on Wireless Sensing, Local Positioning, and RFID*, Cavtat, Croatia, Sep. 2009, pp. 1–6.

[15] A. J. Davison, "Real-time simultaneous localisation and mapping with a single camera." in *Iccv*, vol. 3, 2003, pp. 1403–1410.

[16] B. Benfold and I. Reid, "Stable multi-target tracking in real-time surveillance video," in *CVPR 2011*. IEEE, 2011, pp. 3457–3464.

[17] C. Zhang, M. Kuhn, B. Merkl, M. Mahfouz, and A. E. Fathy, "Development of an UWB indoor 3D positioning radar with millimeter accuracy," in *2006 IEEE MTT-S International Microwave Symposium Digest*, San Francisco, CA, USA, Jun. 2006, pp. 106–109.

[18] R. Mendrzik, H. Wymeersch, and G. Bauch, "Joint localization and mapping through millimeter wave MIMO in 5G systems," in *Proc. 2018 IEEE Global Communications Conference (GLOBECOM)*, Abu Dhabi, UAE, Dec. 2018, pp. 1–6.

[19] Z. Lin, T. Lv, and P. T. Mathiopoulos, "3-D indoor positioning for millimeter-wave massive MIMO systems," *IEEE Transactions on Communications*, vol. 66, no. 6, pp. 2472–2486, Jun. 2018.

[20] A. Guerra, F. Guidi, D. Dardari, A. Clemente, and R. DErrico, "A millimeter-wave indoor backscattering channel model for environment mapping," *IEEE Transactions on Antennas and Propagation*, vol. 65, no. 9, Sep. 2017.

[21] F. Guidi, A. Guerra, D. Dardari, A. Clemente, and R. D'Errico, "Environment mapping with millimeter-wave massive arrays: System design and performance," in *2016 IEEE Globecom Workshops (GC Wkshps)*, Washington, DC, USA, Dec. 2016, pp. 1–6.

[22] O. Kanhere and T. S. Rappaport, "Position locationing for millimeter wave systems," in *Proc. 2018 IEEE Global Communications Conference (GLOBECOM)*, Abu Dhabi, UAE, Dec. 2018, pp. 206–212.

[23] A. Olivier, G. Bielsa, I. Tejado, M. Zorzi, J. Widmer, and P. Casari, "Lightweight indoor localization for 60-GHz millimeter wave systems," in *Proc. 13th Annual IEEE Int. Conf. on Sensing, Communication, and Networking (SECON)*, London, UK, Jun. 2016, pp. 1–9.

[24] P. Park, S. Kim, S. Woo, and C. Kim, "A centimeter resolution, 10 m range CMOS impulse radio radar for human motion monitoring," *IEEE Journal of Solid-State Circuits*, vol. 49, no. 5, pp. 1125–1134, May 2014.

[25] H. J. Ng, W. Ahmad, M. Kucharski, J. Lu, and D. Kissinger, "Highly-miniaturized 2-channel mm-wave radar sensor with on-chip folded dipole antennas," in *Proc. IEEE Radio Frequency Integrated Circuits Symposium (RFIC)*, Honolulu, HI, USA, Jun. 2017, pp. 368–371.

[26] R. Ebelt, A. Hamidian, D. Shmakov, T. Zhang, V. Subramanian, G. Boeck, and M. Vossiek, "Cooperative indoor localization using 24-GHz CMOS radar transceivers," *IEEE Transactions on Microwave Theory and Techniques*, vol. 62, no. 9, pp. 2193–2203, Sep. 2014.

[27] ISO/IEC Guide 98-3:2008, *Uncertainty of measurement – Part 3: Guide to the expression of uncertainty in measurement (GUM:1995)*, Jan. 2008.

[28] T. K. Y. Bar-Shalom, X. Rong Li, *Estimation with Application to Tracking and Navigation – Theory, Algorithm and Software*. John Wiley and Sons, 2001.